SCIENCE CHINA
Earth Sciences

• RESEARCH PAPER •

June 2014 Vol.57 No.6: 1192–1198
doi: 10.1007/s11430-013-4775-2

3D-FEM modeling of the microscopic stress field of forsterite aggregate under hydrostatic pressure: Significance of the crystal orientation

CHEN YuXiang[1,2], LIU Xi[1,2*] & ZHOU YongSheng[3]

[1] *The Key Laboratory of Orogenic Belts and Crustal Evolution, MOE, Peking University, Beijing 100871, China;*
[2] *School of Earth and Space Sciences, Peking University, Beijing 100871, China;*
[3] *The State Key Laboratory of Earthquake Dynamics, Institute of Geology, Earthquake Administration, Beijing 100029, China*

Received April 17, 2013; accepted August 18, 2013; published online February 19, 2014

Three Dimensional Finite Element Method (3D-FEM) has been used to model the deviatoric stress field in a forsterite aggregate with a sandwich geometry: two forsterite cubes aligned in the same crystallographic orientation (the "breads") sandwich a third forsterite cube (the "filling"), which might have an identical or different crystallographic orientation. The results show that there is no von Mises stress in the forsterite sandwich if the sandwiching and sandwiched forsterite cubes are aligned in the same crystallographic orientation. If the crystallographic orientations are different, however, von Mises stress and heterogeneous stress distribution occur both along the boundary and in the forsterite cubes. For the investigated *P-T* conditions (up to 6.4 GPa and 500°C), the resulted deviatoric stress is much lower than the yield strength of forsterite, so that higher *P*, higher *T*, or other means to create higher deviatoric stress is necessary, in order to constrain the yielding behavior of forsterite.

3D-FEM, forsterite aggregate, crystallographic orientation, stress distribution

Citation: Chen Y X, Liu X, Zhou Y S. 2014. 3D-FEM modeling of the microscopic stress field of forsterite aggregate under hydrostatic pressure: Significance of the crystal orientation. Science China: Earth Sciences, 57: 1192−1198 doi: 10.1007/s11430-013-4775-2

Olivine, with its composition close to pure forsterite, is the major mineral in the upper mantle of the Earth (Ringwood, 1975). Its deformation mechanism provides significant insight into the dynamical processes of the Earth's interior (Karato and Wu, 1993). Indeed, its rheological properties have been used to interpret the seismic anisotropy of the upper mantle (Pera et al., 2003; Mainprice et al., 2008; Michibayashi et al., 2006), and are considered as one of the major factors controlling the evolution of the anisotropic viscosity of the upper mantle (Tommasi et al., 2009).

Because of the importance of the rheological properties of olivine, a large number of novel experimental techniques were employed to investigate its yield strength, including measurements of single crystal hardness (Evans and Goetze, 1979), measurements of radial *P* distribution and final sample thickness in a diamond-anvil cell (DAC; Meade and Jeanolz, 1990), measurements of peak broadening of powder X-ray diffraction patterns in a conventional DIA apparatus (Chen et al., 1998; Li et al., 2003), and measurements of macroscopic strain with time-resolved X-ray radiography imaging and microscopic strain with X-ray diffraction in a D-DIA apparatus (Raterron et al., 2009; Girard et al., 2010; Long et al., 2011). These measurements, especially those with the D-DIA (Wang et al., 2003), substantially improved our understanding of the rheological behavior of olivine. For example, the deformation behavior of olivine at subduction zone *P-T* conditions was firmly established recently

*Corresponding author (email: xi_liu@pku.edu.cn)

(Long et al., 2011).

In the measurements of the microscopic strain with the X-ray diffraction technique, there is an assumption that the microscopic deviatoric stresses must be present with their orientation and magnitude distributing randomly, with the exact details unknown though (Weidner et al., 1994a, 1994b). On the other hand, microstructural modeling suggested that grain size, shape, and orientation may lead to significant microscopic stress heterogeneity, and stress concentration might be high enough to cause localized plastic microdeformation even when a polycrystalline aggregate is in its macroscopic elastic regime (Kozaczek et al., 1995; Castelnau et al., 2008). Indeed, stress concentration at grain boundary has been experimentally observed (Li et al., 2003). In order to understand the origin of the deviatoric stress in a compressed olivine aggregate, obviously it is crucial to know the details of the microscopic stress distribution. However, present X-ray diffraction technique cannot achieve the spatial resolution down to the submicron scale.

Here we constructed a simplified model for the forsterite aggregate, and probed its microscopic stress distribution pattern by using a Three Dimensional Finite Element Method (3D-FEM), a method well established and widely used in the materials science (Fallahi and Ataee, 2010; Roters et al., 2010). As will be obvious later, severe deviatoric stress along the grain boundary between two crystals with different crystallographic orientations and strong stress heterogeneity in the grains occur. In addition, the effects of *P* and *T* on the microscopic stress field have been investigated.

1 Experimental details

In the simplified forsterite aggregate model (Figure 1(a)), three forsterite cubes A, B, and C with an edge length of 1 μm were aligned into a sandwich geometry, with Cubes B and C in the same crystallographic orientation. The origin of the 3D Cartesian coordinate system (Point O) was located at the geometric center of the sandwich. The computing unit cell consisted of one fourth of Cube B and one eighth of Cube A. Two boundary conditions were applied: one was the displacement constraint, with the displacement-free planes overlapping with the coordinate planes (Figure 1(a)), and the other was the macroscopic *P* constraint loaded on the external surfaces of the forsterite sandwich. Additionally, friction contact between the cubes was considered, with the friction coefficient along the boundary set as 0.6 (Byerlee, 1978).

Forsterite is orthorhombic (space group *Pbnm*). During its elastic deformation, its microscopic stress (σ_{ij}) and strain (ε_{ij}) can be related via its elastic constant tensor (c_{ij}), as follows (Liebermann et al., 1998):

$$\sigma_{ij} = c_{ij}\varepsilon_{ij}, \tag{1}$$

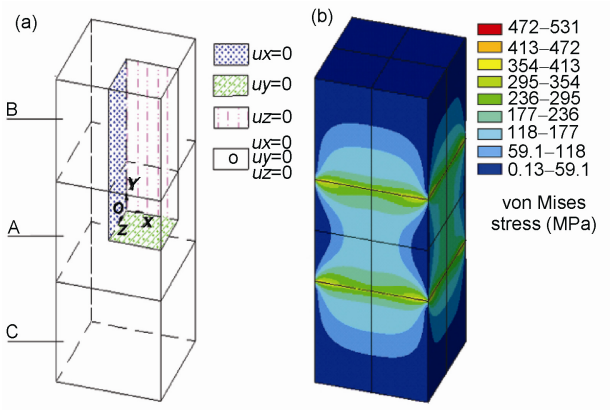

Figure 1 The forsterite sandwich. (a) Arrangement of Cubes A, B and C in the Cartesian coordinate system. Point O is the origin while *ux*, *uy*, and *uz* are the displacements in the *X*-, *Y*-, and *Z*-directions, respectively. The shadowed planes are the coordinate planes, in which the displacements are set as zero. (b) Contour of the von Mises stress field example by Model 18 (1.6 GPa and 500°C; Table 1).

where

$$\sigma_{ij} = \{\sigma_{11}, \sigma_{22}, \sigma_{33}, \sigma_{12}, \sigma_{13}, \sigma_{23}\}, \tag{2}$$

$$\varepsilon_{ij} = \{\varepsilon_{11}, \varepsilon_{22}, \varepsilon_{33}, \varepsilon_{12}, \varepsilon_{13}, \varepsilon_{23}\}, \tag{3}$$

and

$$c_{ij} = \begin{bmatrix} c_{11} & c_{12} & c_{13} & & & \\ c_{12} & c_{22} & c_{23} & & & \\ c_{13} & c_{23} & c_{33} & & & \\ & & & c_{44} & & \\ & & & & c_{55} & \\ & & & & & c_{66} \end{bmatrix}. \tag{4}$$

The elastic constant tensors of forsterite at ambient *P-T* condition and their *P* derivatives and *T* derivatives were taken from Kumazawa and Andenson (Kumazawa and Anderson, 1969). The elastic constant tensors at the *P-T* conditions in interest were calculated by the following equation:

$$c_{ij} = c_{ij}^0 + \frac{\mathrm{d}c_{ij}}{\mathrm{d}P}(P - P_0) + \frac{\mathrm{d}c_{ij}}{\mathrm{d}T}(T - T_0), \tag{5}$$

where c_{ij}, $\mathrm{d}c_{ij}/\mathrm{d}P$ and $\mathrm{d}c_{ij}/\mathrm{d}T$ are the elastic constant tensors at the *P-T* conditions in interest, their *P* derivatives, and *T* derivatives, respectively. c_{ij}^0 is the elastic constant tensors at 1 atm (P_0) and room *T* (T_0). Using the corresponding elastic constant tensors, the Young's moduli (E_{ij}), shear moduli (G_{ij}), and Poisson's ratio (μ_{ij}) in different crystallographic directions of forsterite at different *P-T* conditions, as input data to the modeling, were derived by using the equations outlined in Bucur and Archer (1984).

The 3D-FEM modeling was carried out by using the ANSYS software. The mesh element SOLID 185, especially

for the 3D modeling of solid structures, was adopted to mesh the cubes. The mesh size was 0.02 μm× 0.02 μm× 0.02 μm. The contact and target elements were CONTACT 174 and TARGET 173, respectively. Overall, there were 15625 elements for Cube A, 31250 elements for Cube B, and 52052 nodes in the entire computing model.

The computed microscopic stress field was characterized by using the von Mises stress. As exampled by Figure 1(b), the microscopic stress field in the forsterite sandwich could be severely heterogeneous.

2 Results and discussion

Two sets of experiments have been conducted, with the 1st set designed to evaluate the effect of different crystallographic orientations on the microscopic stress field and the 2nd set to evaluate the effects of macroscopic *P* and *T* (up to 6.4 GPa and 500°C; Tables 1 and 2). For the investigated *P-T* range, the flow mechanism of olivine is dominated by dislocation creep (Li et al. , 2003; Long et al., 2011), so that grain size is not important. However, the shape of the forsterite grains might be a key factor (Kozaczek et al., 1995), but was not considered in this study.

The 1st set of experiments was conducted at 1.6 GPa and 500°C. In total, 18 different crystallographic orientation combinations were identified, but only 15 of them are independent (Table 1; Model 2 = Model 7, Model 3 = Model 13, Model 9 = Model 14).

Figure 2 shows the stress distribution on the top face of Cube A along the Cube A-Cube B boundary. When the crystallographic orientations of Cubes A and B are the same (Models 1, 8 and 15; Table 1), the stress distribution is essentially uniform and the von Mises stress is close to zero.

Table 1 Maximum and minimum von Mises stresses with two forsterite cubes in different crystal orientations (*hkl*) in reference to the Cartesian coordinate system (*X*, *Y*, *Z*)

Alignment of cubes to the Cartesian		Model	Von Mises stress		FWHM (μm)
Cube A	Cube B		Max (MPa)	Min (MPa)	
	[100]//*X*, [010]//*Y*, [001]//*Z*	1	0.0152	5.760×10^{-11}	–
[100]//*X*,	[001]//*X*, [100]//*Y*, [010]//*Z*	2	278.77	0.0438	0.141(6)
[010]//*Y*,	[010]//*X*, [001]//*Y*, [100]//*Z*	3	–	–	–
[001]//*Z*	[001]//*X*, [010]//*Y*, [100]//*Z*	4	268.26	0.0626	0.182(6)
	[010]//*X*, [100]//*Y*, [001]//*Z*	5	374.04	0.2048	0.155(6)
	[100]//*X*, [001]//*Y*, [010]//*Z*	6	164.27	0.0273	0.189(7)
	[100]//*X*, [010]//*Y*, [001]//*Z*	7	–	–	–
[001]//*X*,	[001]//*X*, [100]//*Y*, [010]//*Z*	8	0.0152	1.664×10^{-10}	–
[100]//*Y*,	[010]//*X*, [001]//*Y*, [100]//*Z*	9	412.53	0.0963	0.204(6)
[010]//*Z*	[001]//*X*, [010]//*Y*, [100]//*Z*	10	373.73	0.0980	0.173(6)
	[010]//*X*, [100]//*Y*, [001]//*Z*	11	219.39	0.1062	0.228(9)
	[100]//*X*, [001]//*Y*, [010]//*Z*	12	195.29	0.0466	0.179(6)
	[100]//*X*, [010]//*Y*, [001]//*Z*	13	424.89	0.1253	0.190(6)
[010]//*X*,	[001]//*X*, [100]//*Y*, [010]//*Z*	14	–	–	–
[001]//*Y*,	[010]//*X*, [001]//*Y*, [100]//*Z*	15	0.0152	6.609×10^{-11}	–
[100]//*Z*	[001]//*X*, [010]//*Y*, [100]//*Z*	16	161.99	0.0066	0.197(6)
	[010]//*X*, [100]//*Y*, [001]//*Z*	17	196.33	0.0664	0.165(6)
	[100]//*X*, [001]//*Y*, [010]//*Z*	18	531.11	0.1249	0.196(6)

Table 2 Maximum and minimum von Mises stresses for Model 18 at different *P-T* conditions

P (MPa)	*T* (°C)	von Mises stress		FWHM (μm)
		Max (MPa)	Min (MPa)	
400	500	122.56	0.0301	0.195(6)
800	500	257.19	0.0624	0.195(6)
3200	500	1056.9	0.2378	0.197(6)
6400	500	2065.9	0.4245	0.198(7)
1600	25	519.30	0.1110	0.197(6)
1600	100	514.98	0.1112	0.197(6)
1600	200	512.22	0.1091	0.197(6)
1600	300	526.62	0.1191	0.196(6)
1600	400	527.23	0.1220	0.196(6)

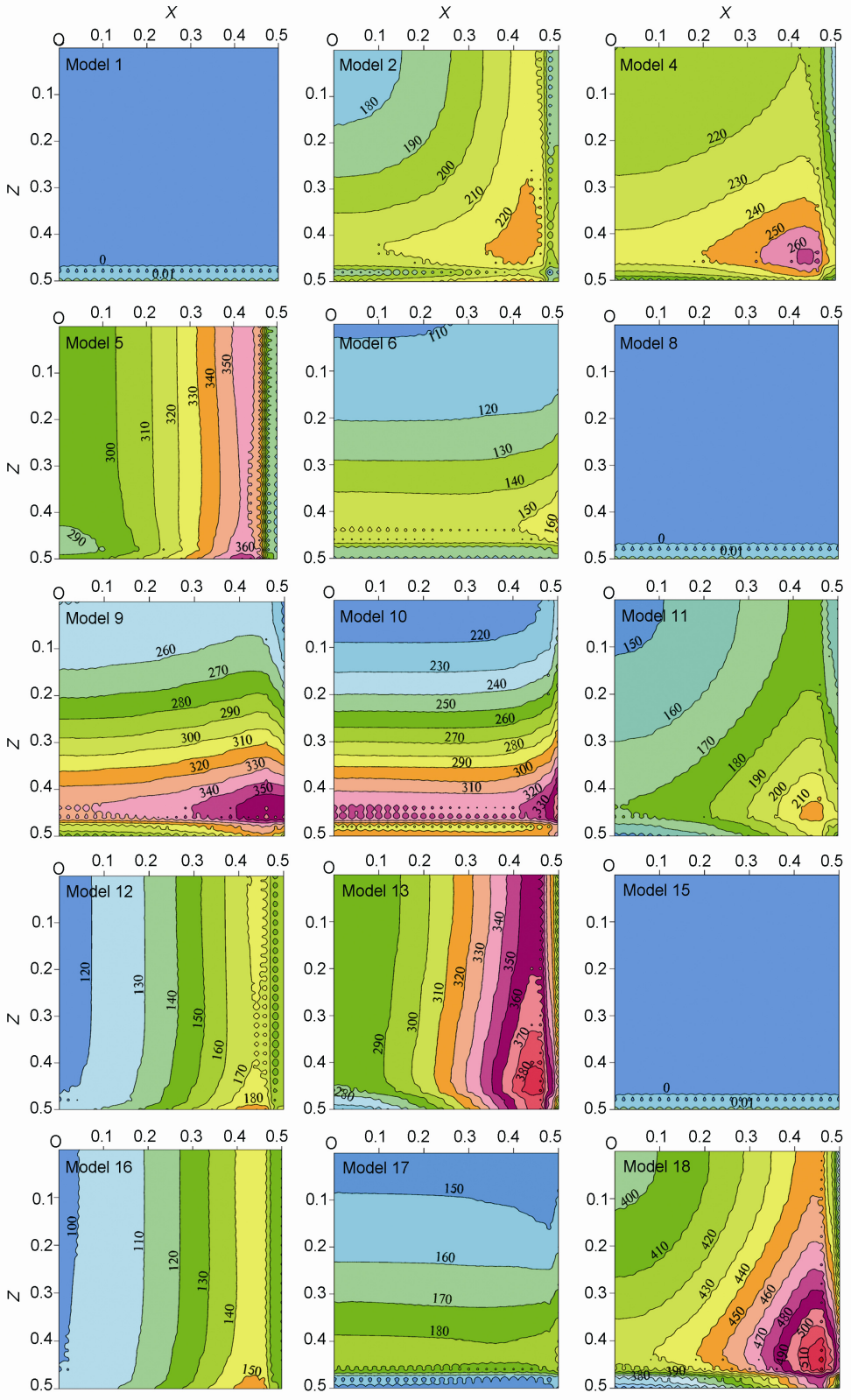

Figure 2 Distribution of the von Mises stress (Ma) on part of the top face of Cube A (Y = 0.5 μm). See Table 1 for the orientations of the cubes. The unit for X and Z is μm.

When the crystallographic orientations are different, however, the stress distribution for any specific model is severely heterogeneous, with the von Mises stress generally attaining its maximum value around the corner (X = 0.5 μm, Z = 0.5 μm) and gradually decreasing towards Point O. There are also large differences in the von Mises stresses

among the models, as manifested by the maximum, minimum and gradient of the von Mises stress; averagely, Model 18 displays the highest von Mises stress. These observations verify the claim that the experimentally observed deviatoric stress is indeed a mean value (Long et al., 2011; Weidner et al., 1994a, 1994b).

Figure 3(a) shows the patterns of the von Mises stresses along the *X*-coordinate. Apparently, different combinations of the crystallographic alignments of the sandwiching and sandwiched forsterite cubes lead to very different magnitudes of the von Mises stresses. As to a specific model, the von Mises stress generally decreases from the edge of the cube (X = 0.5 μm) to the center (X = 0 μm). For all models with Cubes A and B in identical crystallographic orientations, in contrast, the von Mises stress is close to zero.

Figure 3(b) shows the variations of the von Mises stress along the *Y*-coordinate. For all models with Cubes A and B in different crystallographic orientations, the von Mises stress peaks at the boundary position (Y = 0.5 μm), and quickly decreases in both directions away from the boundary. The thickness of the boundary layer, characterized by the full width at half maximum (FWHM; Table 1), varies between 0.141(6) and 0.228(9) μm, with an averaged value of 0.18(2) μm. For the rest three models (Models 1, 8 and 15), on the other hand, no stress peak can be observed, and the von Mises stress is close to zero.

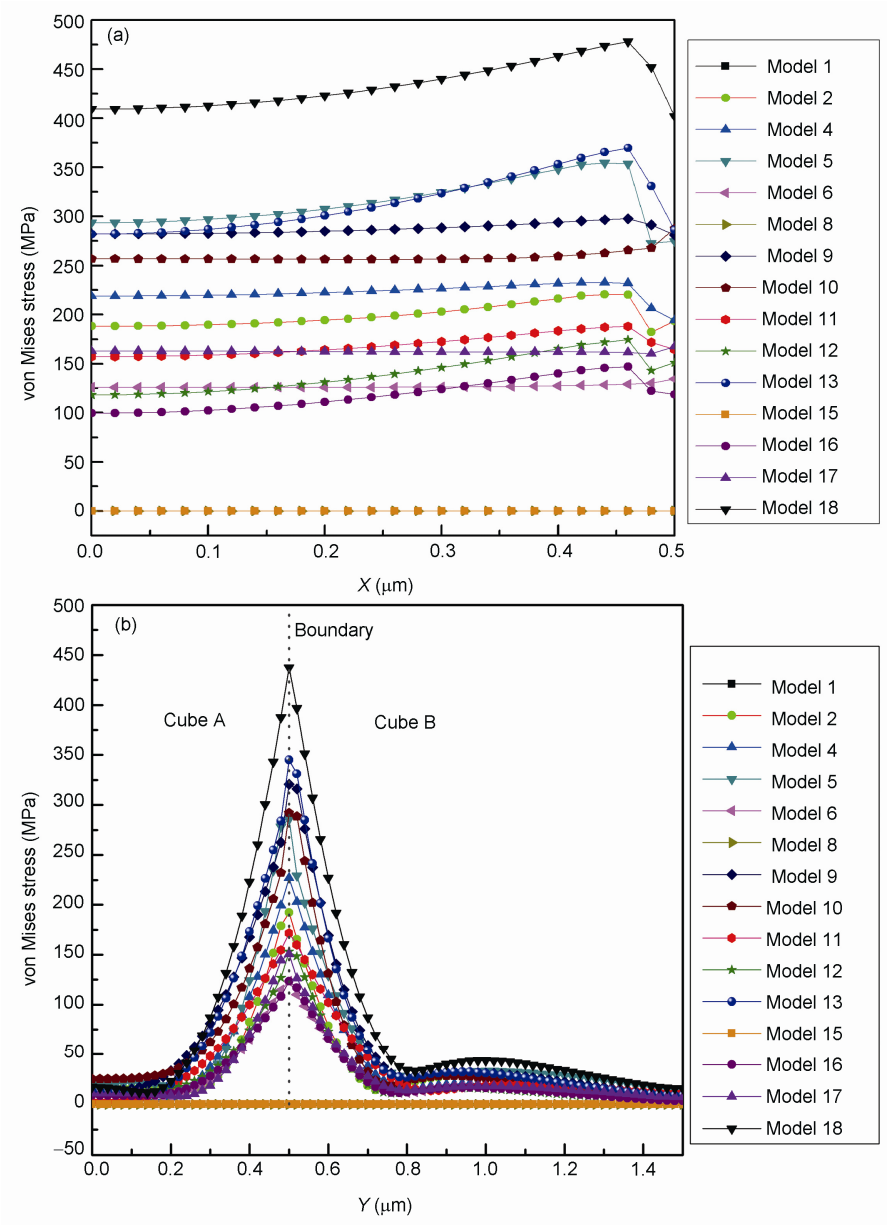

Figure 3 Variations of the von Mises stress along the *X* direction (Y = 0.5 μm and Z = 0.26 μm; Cube A) (a) and along the *Y* direction (X = 0.26 μm and Z = 0.26 μm) (b).

The 2nd set of experiments suggests that for Model 18, the von Mises stress builds up as the macroscopic P goes up (Figure 4(a); 500°C) whereas the microscopic stress field does not vary significantly as T increases (Figure 4(b); 1.6 GPa).

Clearly, our 3D-FEM modeling suggests that due to the elastic anisotropy of forsterite, different crystallographic orientations result in severe deviatoric stress, which is heterogeneously distributed not only among the grains but also in the individual grains. For a macroscopic P of 1.6 GPa, the maximum von Mises stress observed in this study is about 0.531 GPa (Table 1; 500°C), which is much less than the experimentally-determined yield strength of olivine at similar physical conditions (Evan and Goetze, 1979; Meade and Jeanloz, 1990; Chen et al., 1998; Li et al., 2003; Long et al., 2011). To plastically deform olivine, therefore, higher P (Chen et al., 1998; Long et al., 2011), higher T (Weidner et al., 1994b), additional significant stress concentration possibly caused by grain shape (Kozaczek and Goetze, 1995), or different experimental technique (Zhang and Karato, 1995) must be resorted. Furthermore, the maximum von Mises stress caused by different crystallographic orientation of forsterite at 500°C (Model 18; Table 2) is approximately one third of the macroscopic loading P, which is significantly less pronounced than that of diamond; in the latter case, the deviatoric stress that can be generated by the direct compression was about twice the loading P (Weidner et al., 1994b).

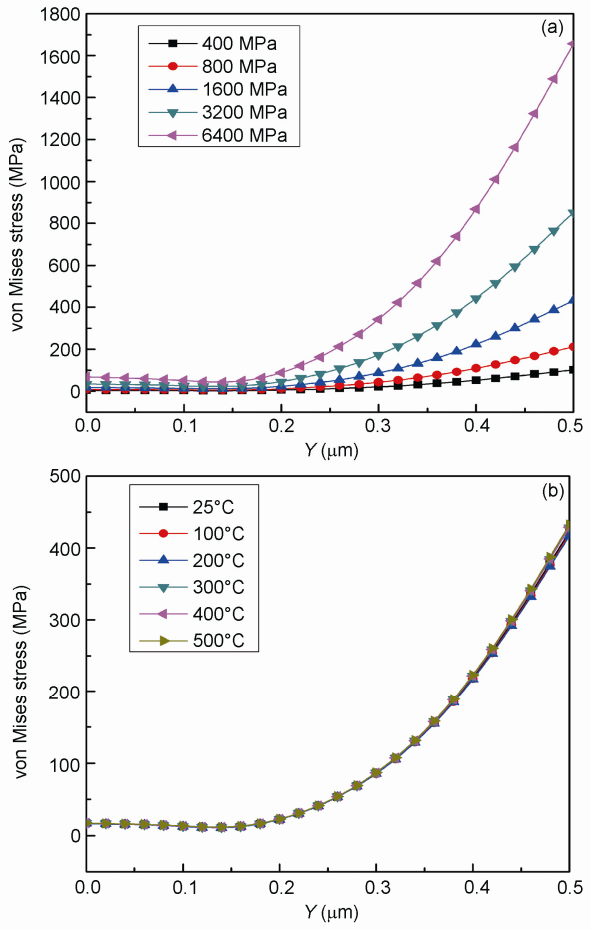

Figure 4 Effects of P (a) and T (b) on the von Mises stress along the Y direction (X = 0.26 μm and Z = 0.26 μm; Model 18).

The intense deviatoric stress brought forth by the different crystallographic orientations of the olivine grains, especially along their boundaries (Figure 3(b)), has the potentials to explain their boundary layer's reservoir effect of incompatible elements (Hiraga et al., 2004). Due to the distinct difference in the stress states between the boundary layers and internal portions of the olivine grains, their unit-cell parameters should be rather different, which might lead to different capabilities in hosting the incompatible elements, as suggested by the lattice strain model (Blundy et al., 1994).

3 Conclusions

Our 3D-FEM modeling suggests that:

(1) The forsterite sandwich shows no von Mises stress if the sandwiching and sandwiched forsterite cubes are aligned in the same crystallographic orientation.

(2) The forsterite sandwich shows significant von Mises stress and heterogeneous stress distribution both along the boundary and in the forsterite cubes if the forsterite cubes are aligned in different crystallographic orientations.

(3) For the investigated P-T conditions (up to 6.4 GPa and 500°C), the resulted deviatoric stress is much lower than the yield strength of forsterite though. In order to constrain the yielding behavior of forsterite, higher P, higher T or other means to create higher deviatoric stress is a prerequisite.

This research was supported by National Natural Science Foundation of China (Grant No. 41090371).

Blundy J D, Wood B J. 1994. Prediction of crystal-melt partition coefficients from elastic moduli. Nature, 372: 452–454

Bucur V, Archer R R. 1984. Elastic constants for wood by an ultrasonic method. Wood Sci Technol, 18: 255–265

Byerlee J. 1978. Friction of rocks. Pure Appl Geophys, 116: 615–626

Castelnau O, Blackman D K, Lebensohn R A, et al. 2008. Micromechanical modeling of the viscoplastic behavior of olivine. J Geophys Res, 113: B09202

Chen J, Inoue T, Weidner D J, et al. 1998. Strength and water weakening of mantle minerals, olivine, wadsleyite and ringwoodite. Geophys Res Lett, 25: 575–578

Evans B, Goetze C. 1979. The temperature variation of hardness of olivine and its implication for polycrystalline yield stress. J Geophys Res, 84: 5505–5524

Fallahi A, Ataee A. 2010. Effects of crystal orientation on stress distribution near the triple junction in a tricrystal γ-TiAl. Mater Sci Eng A, 527: 4576–4581

Girard J, Chen J, Raterron P, et al. 2010. Deformation of single crystal sample using D-DIA apparatus coupled with synchrotron X-rays: *In situ* stress and strain measurements at high pressure and temperature. J

Phys Chem Solids, 71: 1053–1058
Hiraga T, Anderson I M, Kohlstedt D L. 2004. Grain boundaries as reservoirs of incompatible elements in the Earth's mantle. Nature, 427: 699–703
Karato S, Wu P. 1993. Rheology of the upper mantle: A synthesis. Science, 260: 771–778
Kozaczek K J, Petrovic B G, Ruud C O, et al. 1995. Microstructural modeling of grain-boundary stresses in Alloy 600. J Mater Sci, 30: 2390–2400
Kumazawa M, Anderson O L. 1969. Elastic moduli, pressure derivatives, and temperature derivatives of single-crystal olivine and single-crystal forsterite. J Geophys Res, 74: 5961–5972
Liebermann R C, Li B. 1998. Elasticity at high pressures and temperatures. In: Hemley R J, ed. Ultrahigh Pressure Mineralogy: Physics and Chemistry of the Earth's Deep Interior. Rev Mineral, 37: 459–492
Li L, Raterron P, Weidner D, et al. 2003. Olivine flow mechanisms at 8 GPa. Phys Earth Planet Inter, 138: 113–129
Long H, Weidner D J, Li L, et al. 2011. Deformation of olivine at subduction zone conditions determined from *in situ* measurements with synchrotron radiation. Phys Earth Planet Inter, 186: 23–35
Mainprice D, Tommasi A, Ferré D, et al. 2008. Predicted glide systems and crystal preferred orientations of polycrystalline silicate Mg-Perov- skite at high pressure: Implications for the seismic anisotropy in the lower mantle. Earth Planet Sci Lett, 271: 135–144
Meade C, Jeanloz R. 1990. The strength of mantle silicates at high pressures and room temperature: Implications for the viscosity of the mantle. Nature, 348: 533–535
Michibayashi K, Abe N, Okamoto A, et al. 2006. Seismic anisotropy in the uppermost mantle, back-arc region of the northeast Japan arc: Petrophysical analyses of Ichinomegata peridotite xenoliths. Geophys Res Lett, 33: L10312
Pera E, Mainprice D, Burlini L. 2003. Anisotropic seismic properties of the upper mantle beneath the Torre Alfina area (Northern Apennines, Central Italy). Tectonophysics, 370: 11–30
Raterron P, Amiguet E, Chen J, et al. 2009. Experimental deformation of olivine single crystals at mantle pressures and temperatures. Phys Earth Planet Inter, 172: 74–83
Ringwood A E. 1975. Composition and Petrology of the Earth's Mantle. New York: McGraw-Hill
Roters F, Eisenlohr P, Hantcherli L, et al. 2010. Overview of constitutive laws, kinematics, homogenization and multiscale methods in crystal plasticity finite-element modeling: Theory, experiments, applications. Acta Mater, 58: 1152–1211
Tommasi A, Knoll M, Vauchez A, et al. 2009. Structural reactivation in plate tectonics controlled by olivine crystal anisotropy. Nat Geosci, 2: 423–427
Wang Y, Durham W B, Getting I C, et al. 2003. The deformation-DIA: A new apparatus for high temperature triaxial deformation to pressures up to 15 GPa. Rev Sci Instrum, 74: 3002–3011
Weidner D J, Wang Y, Vaughan M T. 1994a. Yield strength at high pressure and temperature. Geophys Res Lett, 21: 753–756
Weidner D J, Wang Y, Vaughan M T. 1994b. Strength of diamond. Science, 266: 419–422
Zhang S, Karato S. 1995. Lattice preferred orientation of olivine aggregates deformed in simple shear. Nature, 375: 774–777